RESEARCH ARTICLE

NANO · MICRO small
www.small-journal.com

Defect Engineering of Metal Halide Perovskite Nanocrystals via Spontaneous Diffusion of Ag Nanocrystals

Sanghyun Jeon, Junhyuk Ahn, Myung-Chul Jung, Ho Kun Woo, Junsung Bang, Byung Ku Jung, Seongkeun Oh, Sang Yeop Lee, Kyu Joon Lee, Taejong Paik, Don-Hyung Ha, Jae-Pyoung Ahn, Sohee Jeong, Dong Hoe Kim, Jun Hong Noh, Ho Seong Jang, Myung Joon Han,* and Soong Ju Oh**

Perovskite nanocrystals (NCs) have emerged as a promising building block for the fabrication of optic-/optoelectronic-/electronic devices owing to their superior characteristics, such as high absorption coefficient, rapid ion mobilities, and tunable energy levels. However, their low structural stability and poor surface passivation have restricted their application to next-generation devices. Herein, a drug delivery system (DDS)-inspired post-treatment strategy is reported for improving their structural stability by doping of Ag into $CsPbBr_3$ (CPB) perovskite NCs; delivery to damaged sites can promote their structural recovery slowly and uniformly, averting the permanent loss of their intrinsic characteristics. Ag NCs are designed through surface-chemistry tuning and structural engineering to enable their circulation in CPB NC dispersions, followed by their delivery to the CPB NC surface, defect-site recovery, and defect prevention. The perovskite-structure healing process through the DDS-type process (with Ag NCs as the drug) is analyzed by a combination of theoretical calculations (with density functional theory) and experimental analyses. The proposed DDS-inspired healing strategy significantly enhances the optical properties and stability of perovskite NCs, enabling the fabrication of white light-emitting diodes.

1. Introduction

Perovskite nanocrystals (NCs) hold significant potential as fundamental components in the development of next-generation optoelectronic devices, including solar cells, displays, and image sensors.[1–5] This potential stems from their exceptional optical and electrical properties, including high absorption coefficients, tunable bandgaps, and excellent carrier mobility.[3,6–8] Despite these outstanding characteristics, the practical applicability of the material has been limited by its inherent instability, primarily resulting from the prevalence of intrinsic defects.[9–14] To address this challenge, researchers have investigated several defect passivation strategies, including hybridization with organic cations, alkali–metal doping, and surface ligand modifications.[15–18] Among strategies such as alloying, surface modifications, and core–shell formation, the doping techniques (with Ag, Mn,

S. Jeon, J. Ahn, H. K. Woo, J. Bang, B. K. Jung, S. Oh, S. Y. Lee, D. H. Kim, S. J. Oh
Department of Materials Science and Engineering
Korea University
Seoul 02841, Republic of Korea
E-mail: sjoh1982@korea.ac.kr

M.-C. Jung, M. J. Han
Department Physics
Korea Advanced Institute of Science and Technology
Daejeon 34141, Republic of Korea
E-mail: mj.han@kaist.ac.kr

K. J. Lee, J.-P. Ahn
Advanced Analysis Center
Korea Institute of Science and Technology
Seoul 02792, Republic of Korea

T. Paik, D.-H. Ha
School of Integrative Engineering
Chung-Ang University
Seoul 06974, Republic of Korea

S. Jeong, H. S. Jang
Materials Architecturing Research Center
Korea Institute of Science and Technology
Seoul 02792, Republic of Korea
E-mail: msekorea@kist.re.kr

J. H. Noh
School of Civil
Environmental and Architectural Engineering
Korea University
Seoul 02841, Republic of Korea

J. H. Noh
KU-KIST Green School Graduate School of Energy and Environment
Korea University
Seoul 02841, Republic of Korea

J. H. Noh
Department of Integrative Energy Engineering
Korea University
Seoul 02841, Republic of Korea

The ORCID identification number(s) for the author(s) of this article can be found under https://doi.org/10.1002/smll.202307032

DOI: 10.1002/smll.202307032

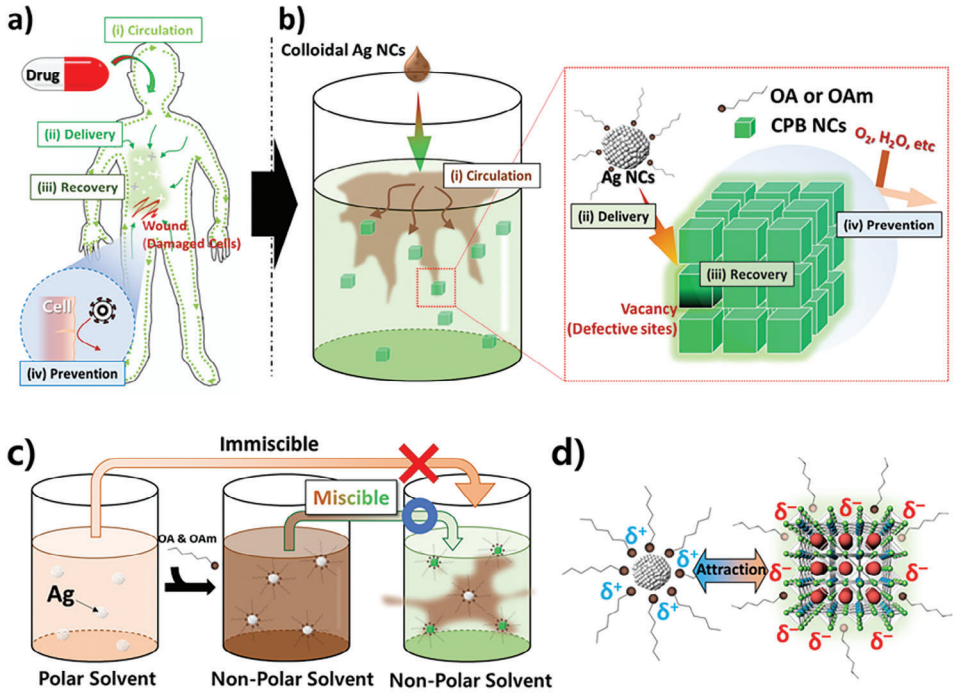

Figure 1. Schematic illustration of a) drug delivery system (DDS)-based wound-healing in the human body, and b) defect-passivation in $CsPbBr_3$ (CPB) perovskite NCs via a DDS-type system (involving circulation, delivery, and recovery) using Ag NCs (as the drug). Schematic illustration of the c) miscibility of Ag NCs, according to the chemical nature of the solvent, and d) electrical forces of attraction between the Ag and CPB NCs.

Co, Zn, etc.) have shown high potential for improving structural stability, as well as engineering characteristics, by passivating defect sites.[19–22] Despite numerous research endeavors, the issue of defects has not been fully resolved, and has continued to restrict both material stability and device fabrication. Consequently, there is an urgent need for novel strategies at a fundamental level to eliminate and passivate defects in perovskite NCs.

A drug delivery system (DDS) is a groundbreaking post-treatment method designed to transport drugs precisely to damaged sites in the human body.[23–26] This approach is crucial for curing damaged organics and has emerged through the integration of diverse disciplines, finding widespread use in modern therapeutic practices. Specifically, engineered drugs intended for DDSs play a vital role in i) circulating through the body, ii) delivering medication to precise locations (damaged sites), iii) aiding in the recovery process, and iv) preventing infections or abnormal conditions (**Figure 1**a).[26,27] Despite its critical role and efficiency, this post-treatment strategy has rarely been applied to anything other than the human body, especially in the context of materials.

In this study, we applied DDS-inspired post-treatment into materials science and engineering for the first time, focusing on $CsPbBr_3$ (CPB) perovskite NCs. Specifically, we demonstrated that colloidal silver nanocrystal (Ag NC) can be used as a drug for passivating defect sites in colloidal CPB NC. To enable their participation in i) circulation, ii) delivery, iii) recovery, and iv) prevention processes in the perovskite system, the surface chemistry and structure of the Ag NCs were modified. Theoretical calculations using the density functional theory (DFT), Hume–Rothery rule, and electronic configuration, as well as empirical investigations, including optical, structural, and chemical analyses, were used to investigate the mechanism of the DDS-inspired healing process. The proposed healing strategy significantly improved the optical properties and stability of colloidal dispersions of the CPB perovskite system and enhanced the oxidation and moisture resistance of the perovskite NCs. Additionally, high-performance white light-emitting diodes (WLEDs) were fabricated using the proposed DDS and anion exchange. The proposed cutting-edge technology, which applies drug delivery methods used in pharmacology to materials science applications, significantly improves the structure and properties of CPB perovskite NCs and is expected to revolutionize research on materials science and technology.

2. Results and Discussion

To realize a DDS-based strategy, similar to the technique used in therapeutics, we selected Ag NCs, based on DFT simulations and prediction of Hume–Rothery and electron-configuration-theory. They indicate that Ag can passivate the trap sites in perovskite structures via monovalent substitution.[14,28] Therefore, as shown in Figure 1a,b, Ag NCs were selected as the drug; their surface chemistry was modified for DDS applications.[9,29,30] To facilitate efficient circulation, as the first step of a DDS-type process, the drug material should be well dispersed in the same medium. CPB NCs are dispersed in non-polar solvents; therefore, the Ag NCs were encapsulated in hydrophobic ligands, namely, oleic acid (OA) and oleylamine (OAm), to ensure their dispersal in the

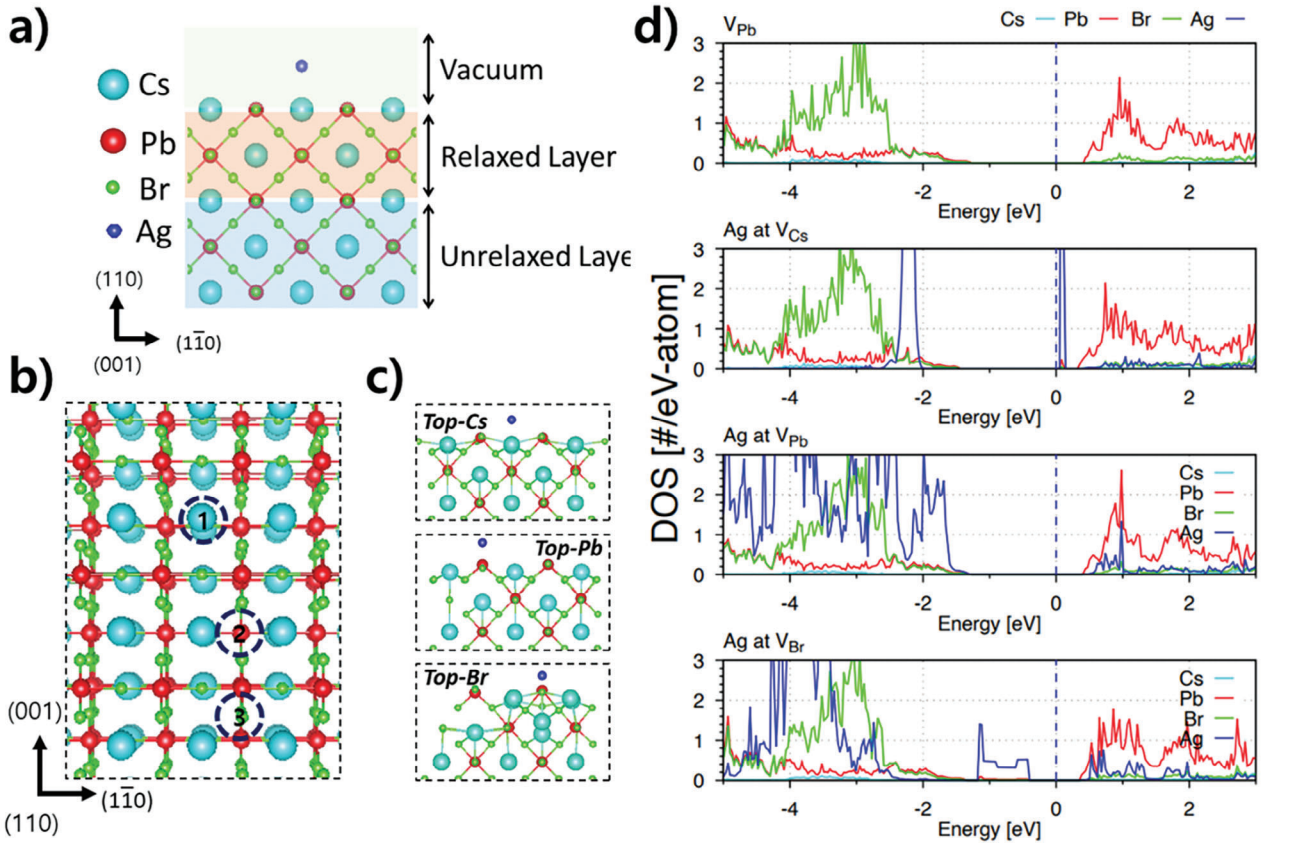

Figure 2. a) A theoretical model structure for CPB (110) surface simulations. b,c) Three candidate absorption sites of the Ag atom; the site 1, 2, and 3 refers to the one on top of Cs, Pb, and Br, respectively. d) The calculated projected density of states of CPB with different Pb vacancy configurations. From the top to the bottom panel, presented are the results of Pb vacancies, Ag filling Cs vacancy sites, Ag filling Pb vacancy sites, and Ag filling Br vacancy sites, respectively. Cyan, red, green, and blue colored lines represent the Cs, Pb, Br, and Ag components, respectively.

CPB NC dispersions (Figure 1c). As the second step of a DDS-type process, the drug material should be efficiently transported to the target sites. Generally, the surface of CPB NCs is negatively charged (−16.0 mV), due to its Br-dominant and/or Pb-defective nature (Figure S1, Supporting Information).[3,31] A small amount of surfactant was added to the Ag NCs, which acted as a reducing and stabilizing agent for the Ag precursor, to generate Ag NCs with a positively charged surface (≈3.4 mV). These modified Ag NCs are attracted to the negatively charged CPB NCs. Additionally, the high surface energy and ion mobility of the Ag NCs facilitated their self-dissociation into Ag ions, and subsequent diffusion into CPB NC vacancies, facilitating their delivery to the target (Figure 1d).[32] For efficient recovery, another vital step of a DDS-type process, the drug should heal the damaged sites. Vacancies in CPB NCs induce in-gap trap states; according to theoretical calculations, Ag ions from the Ag NCs effectively fill Pb vacancies in CPB NCs and passivate the trap states.[6,33,34] Therefore, for prevention, Ag ion passivation was used to design clean, charge-balanced, and ligand-packed CPB NC surface states, to stabilize the colloidal perovskite NCs.

The colloidal CPB NCs and Ag NCs were synthesized by slightly modified wet-chemical methods; details are provided in the Experimental Section.[35,36] During analysis, cuboid CPB NCs with a size of 9 nm and spherical Ag NCs with a size of 4 nm were first dispersed in the non-polar solvents hexane and octane, respectively. Subsequently, CPB-Ag mixtures were prepared by adding Ag NC dispersions (10 mg mL^{-1}) into CPB NC dispersions (10 mg mL^{-1}) in a 5:1 molar ratio at room temperature and under atmospheric conditions. The structure and properties of these CPB-Ag NC mixtures were monitored as a function of time, to investigate the influence of the Ag NCs on CPB NC healing; the CPB-Ag NC mixtures after 1, 3, and 5 days were labeled CPB-Ag (1d), (3d), and (5d) NCs, respectively.

First-principles theoretical calculations were performed within DFT to investigate the proposed delivery-and-recovery mechanism. The results are summarized in **Figure 2** and the computation details are provided in Experimental Section. With a $\sqrt{2} \times \sqrt{2} \times 2$ supercell model for the CPB (110) surface (Figure 2a), which is CsPbBr-terminated showing higher polarity, we calculated total energies and electronic structures corresponding to several different geometric configurations. To identify the favorable surface interaction site for Ag atoms representing the delivery process, three different configurations were considered (Figure 2b,c). The result of DFT total energies demonstrates that Br is the preferred adsorption site. The configuration of Ag locating on top of Br is energetically more stable than that of Cs and Pb by 1.30 and 0.46 eV Ag^{-1}, respectively. Note that the different adsorption configurations lead to different electronic properties

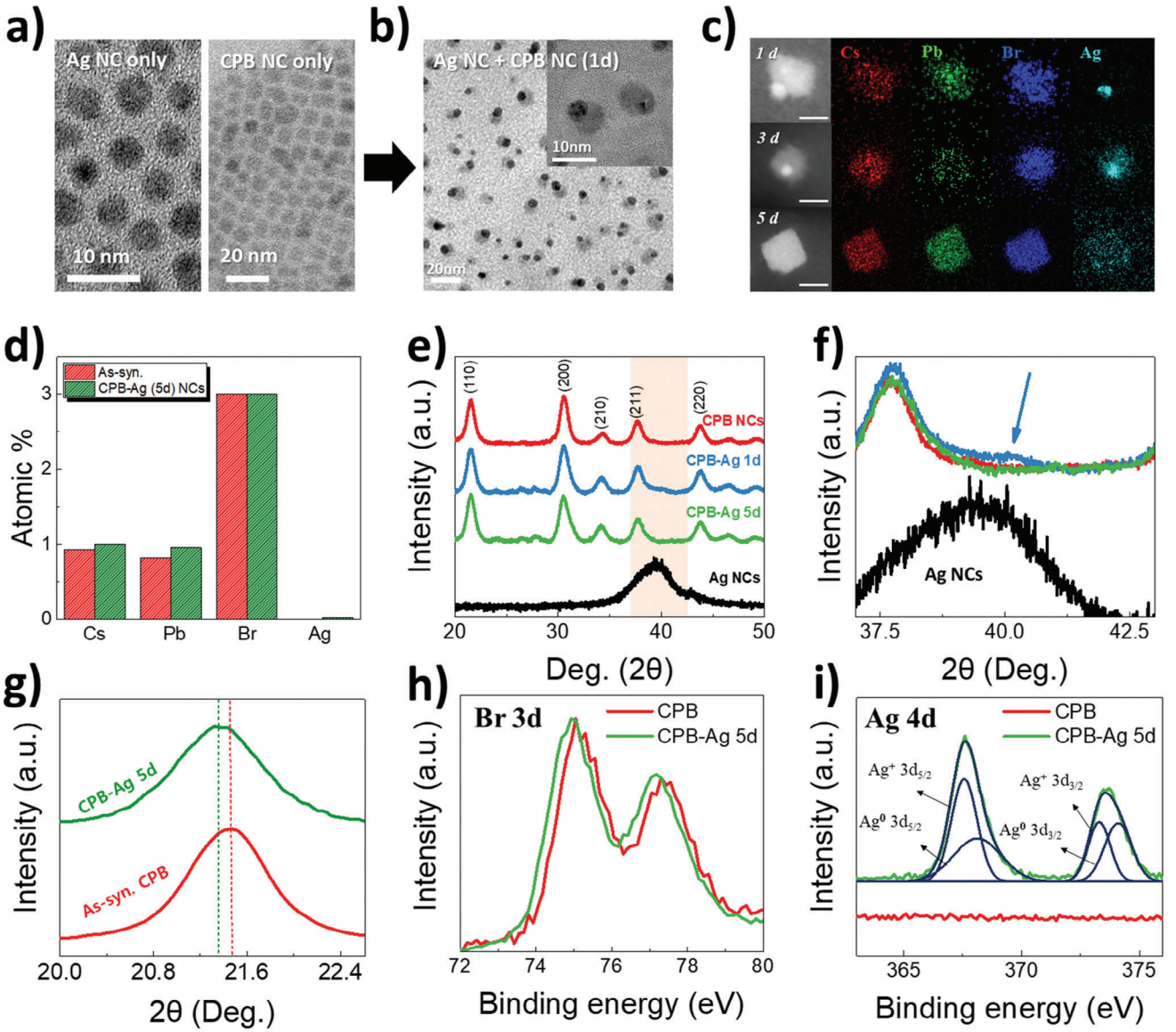

Figure 3. HR-TEM images of the as-synthesized a) Ag NCs (left), CPB NCs (right), and b) CPB-Ag (1d) NCs. c) Scanning-TEM images and scanning-TEM-EDX mapping images of a single CPB-Ag NC after 1, 3, and 5 days (Ag NCs are shown in bright-gray and CPB NCs are shown in dark-gray; red = Cs, green = Pb, blue = Br, and cyan = Ag) (scale bar = 5 nm). d) EDX plots of Cs, Pb, Br, and Ag. e) XRD patterns of the CPB, CPB-Ag (1d), and CPB-Ag (5d) NCs (the abbreviation of as-syn. is as-synthesized). f,g) High-resolution XRD patterns (blue arrow represents Ag NCs). h) Br 3d (68.0 eV), and i) Ag 4d XPS profiles of the CPB and CPB-Ag (5d) NCs.

as discussed in Discussion S1 and Figure S2 (Supporting Information).

The formation energies of Cs, Pb, and Br vacancies were found to be 0.34, 0.22, and 0.77 eV, respectively, indicating that Pb vacancy is most likely. Considering their formal charges, the energy gets reduced to the greatest extent by having Ag atoms on Pb sites. It is consistent with the Ag diffusion and the recovery process discussed above. The corresponding electronic structures are presented in Figure 2d. It is noted that different vacancy configurations give rise to different electronic structures and bandgap value, naturally leading to different optical property. Of our main interest is the Pb vacancy case (the third panel) in which the valence band maximum (VBM) slightly increases. Given that there is no in-gap state and localized state, the sliver gets hybridized well with the mother CPB complex. Our simulation supports the interpretation that Ag was delivered to the CPB surface and spontaneously filled up the vacant Pb sites, being consistent with the healing mechanism of DDSs in the human body.

To empirically investigate the DDS-inspired mechanism proposed here, the structures of the Ag, CPB, and CPB-Ag NCs were investigated; their high-resolution transmission electron microscope (HR-TEM) images are shown in **Figure** 3a,b. The Ag NCs were spheres, while the CPB NCs were distorted rectangles. The distorted cubic structure of the CPB NCs could be attributed to defect sites.[10] On mixing the Ag NCs with CPB NCs, most of

the Ag NCs were found to be attached to the CPB NCs, possibly due to the oppositely charged surfaces, as mentioned in Figure S1, Supporting Information). Additionally, changes in the shape and structure of the CPB-Ag NCs were monitored as a function of time, using TEM and energy dispersive X-ray (EDX) images (Figure 3c). After mixing the Ag and CPB NCs (the as-mixed CPB-Ag NCs are shown in Figure S3, Supporting Information), samples for structural analysis were extracted after 1, 3, and 5 days (Figure S4, Supporting Information). On day 1, Ag NCs with a size of 4 nm were attached to the CPB NCs. On day 3, Ag NCs with half the initial size were observed, possibly due to disassembly. Interestingly, on day 5, no Ag NCs were observed; however, EDX mapping indicates elemental Ag in the entire CPB NC. This implies that Ag was released from the Ag NCs and diffused into the CPB NCs (Figure 3d). On mixing the Ag and CPB NCs, the ratio of Cs:Pb:Br:Ag in the CPB NCs changed from 0.93:0.81:3.00:0.00 to 1.00:0.96:3.00:0.03, and more importantly, the shape of the CPB NCs became more ordered (cubic shape with clean-edged surfaces). The morphology changes may be attributed to the fact that the lattice stress is released by filling the vacancies with Ag ions or atoms, decreasing surface energy and neutralizing unbalanced changes (Figure S1, Supporting Information).[10]

Structural changes of the CPB NCs were monitored, to investigate the Ag diffusion, using X-ray diffraction (XRD) and 2D grazing-incidence wide-angle scattering (GI-WAX), as shown in Figure 3e–g and Figure S5 (Supporting Information). Unlike the spectrum of the CPB NCs, that of the CPB-Ag (1d) NCs contained a slight bump in the range of 38°–40° (indicated by a blue arrow), indicating Ag NCs. After 5 days, the broad peak corresponding to Ag NCs completely disappeared, consistent with the TEM analysis (Figure 3c). After Ag diffusion, most of peaks in the spectrum of the CPB-Ag (5d) NCs were slightly shifted to a lower angle. Changes in the peak center indicate a substitutional diffusion of Ag into CPB NC vacancies, with a slight reduction of the pseudo-orthorhombic phase, as predicted by DFT calculations. Additionally, GI-WAXS measurements of the CPB-Ag (5d) NCs indicated the q values of the (100) and (111) planes, without any other peaks corresponding to distorted structures; this has been described in Discussion S2 (Supporting Information).

X-ray photoemission spectroscopy (XPS) was used to investigate the Ag diffusion further, by monitoring the chemical shifts of perovskite. The XPS spectra (Br 3d and Ag 4d) of as-synthesized- and CPB-Ag (5d) NCs are illustrated in Figure 3g,h (Cs 3d and Pb 4f are presented in Figure S6, Supporting Information). In the CPB-Ag (5d) NC spectrum, the perovskite-related elements (Cs, Pb, and Br) showed slightly lower binding energies than those in the unmodified CPB NCs. Moreover, two strong peaks corresponding to the Ag^+ ion and metal Ag^0 were observed in the Ag 3d spectrum of the CPB-Ag (5d) NCs (Figure 3h). The negative shift of the Pb 4f and Br 3d spectral peaks of the CPB-Ag NCs could be attributed to the low electronegativity of Ag, which induced an electron-density increment of the base element, lowering the binding energy.[37–40] Thus, structural and chemical analyses indicated the diffusion of Ag NCs into the CPB NCs via ionization.

As shown in **Figure** 4a, changes in the optical properties of the colloidal Ag, CPB, and CPB-Ag NCs, as a function of time, were monitored. For the Ag NCs, no color changes were observed with time; they remained brown color, even after 5 days. Contrarily, the colloidal CPB NCs gradually became opaque, underwent agglomeration, and formed a yellow bulk within 4 days. After 5 days, all the substances in the CPB NCs dispersion subsided to the bottom of the vessel, due to agglomeration and sintering; this could be attributed to the inherent instability of colloidal dispersions of CPB NCs. Due to the ionic nature of CPB NCs, they undergo growth and agglomeration in the colloidal state, to reduce their surface energy. Notably, the CPB-Ag NCs showed gradient color changes from bright brown to bright green with time. After 5 days, the color of the mixture was restored to that of its initial state, similar to the as-synthesized CPB NCs. The trend of the color-change recovery corresponded to the structural recovery, as shown in Figure 3c. Notably, the CPB-Ag NCs maintained their transparency and bright-green color, even after a month. Similar trends were observed in the UV–vis spectroscopy results (Figure 4b). The peak representing localized surface plasmonic resonance (LSPR) at 423 nm remained unchanged with time in the Ag NCs spectrum, while it gradually decreased in the CPB NCs spectrum. In the CPB-Ag NC spectrum, the LSPR peak gradually disappeared with time, while the absorbance peak representing CPB perovskites remained unchanged over 5 days.

As shown in Figure 4c, the luminescence was analyzed to investigate the recovery of trap sites. The as-synthesized CPB NCs showed photoluminescence (PL) at 506 nm, which gradually red-shifted and decreased to almost zero over time. The CPB-Ag NCs show red-shifted peak at 514.4 nm at 1d with reduced intensity. After 5 days, the CPB-Ag NCs show enhanced PL intensity, which is 1.2 times higher than that of as-synthesized CPB NCs. Peak position was also not changed after 5 days in CPB-Ag NCs, implying good stability. Then, lifetime data and quantum yield (QY) values were used to elucidate the improved and recovered luminescent properties of the specimen. Time-resolved PL measurements were used to estimate the lifetime of the excited carriers (Figure 4d); the lifetimes of the as-synthesized, as-synthesized (5d), CPB-Ag (1d), and CPB-Ag (5d) NCs were 2.49, 2.01, 2.24, and 2.52 ns, respectively. On day 1 of Ag NC mixing, the lifetime of the Ag-treated CPB NCs was shorter than that of the as-synthesized CPB NCs; however, with time, the former became longer than the latter. As shown in Figure 4e, the as-synthesized CPB NCs exhibited a PL-QY value of 72.5%. The PL-QY was quenched immediately after adding Ag NCs and gradually increased to 74.6% on day 5. This indicates a structure-recovery of the CPB NCs on treatment with Ag NCs, similar to the recovery of the human body on drug treatment in pharmacotherapy.

As shown in **Figure 5**, the electronic structure of the CPB and CPB-Ag (5d) NCs were used to interpret a key element in the proposed DDS-inspired remedy. Figure 5a shows the Tauc plot of the corresponding absorption measurements, along with a line indicating the approximate band edge. The optical bandgaps of the as-synthesized CPB and CPB-Ag (5d) NCs were 2.48 and 2.41 eV, respectively. Subsequently, the energy levels of as-synthesized CPB and CPB-Ag (5d) NC thin films were measured using UV photoelectron spectroscopy (UPS). The Fermi level for the CPB and CPB-Ag (5d) NCs were estimated to be at −4.36 and −5.64 eV, respectively, their VBM values were −4.17 and −5.56 eV,

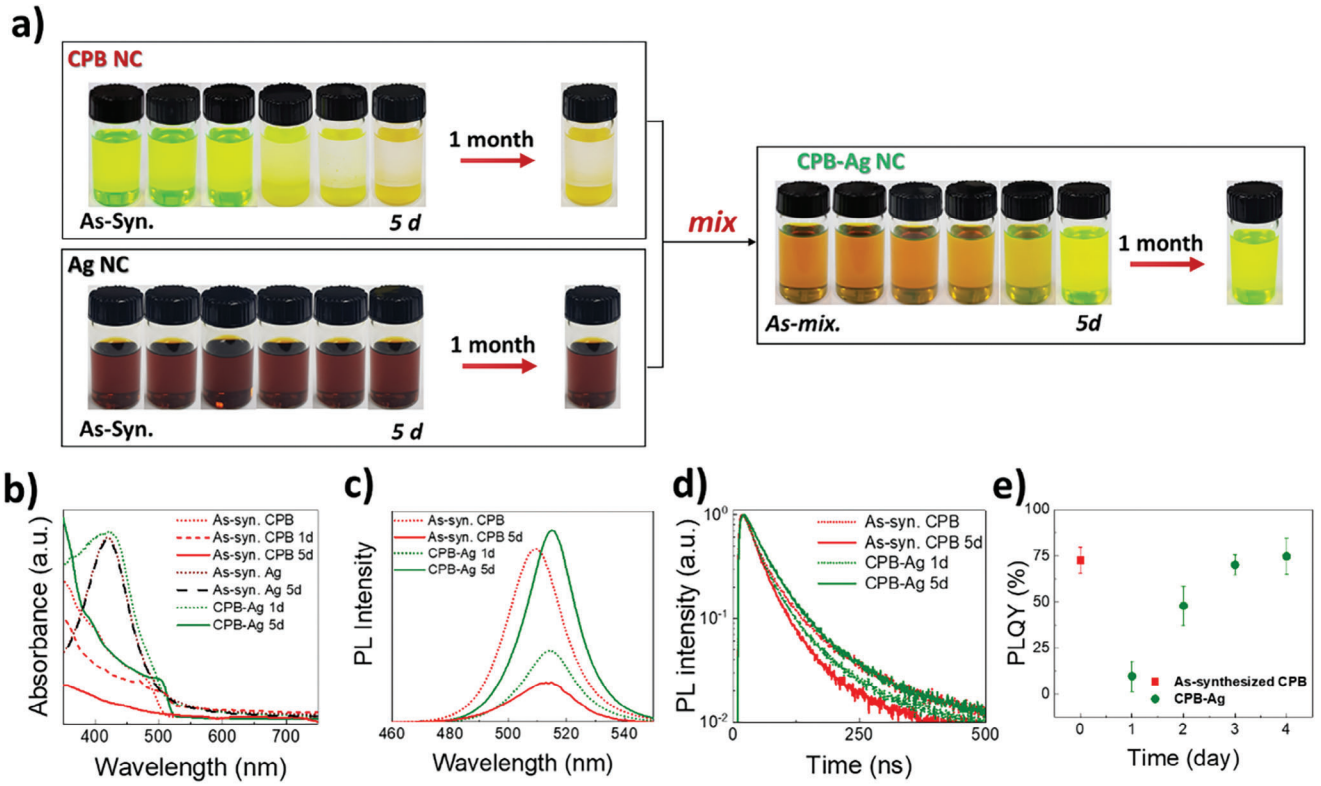

Figure 4. a) Effect of mixing colloidal Ag NC and CPB NC solutions, and a schematic illustration of the doping process. b) Absorbance spectra of the as-synthesized Ag NCs (black dotted line) and CPB NCs (red short-dotted line), CPB NCs after 1 day (red short-dash line) and 5 days (red straight line), and CPB-Ag NCs after 1 day (dark green short-dot line) and 5 days (dark green straight line). c) PL intensity of the CPB, CPB-Ag, and CPB-Ag NCs. Plots of the d) time-resolved photoluminescence (PL) and e) photoluminescence-quantum yields (PL-QYs) of the Ag-mixed CPB NCs versus time.

respectively (Figure 5b,c), and conduction band minimum values were −3.16 and −3.15 eV, respectively. Thus, the CPB-Ag (5d) NCs showed a significantly different VBM energy level compared to that of the CPB NCs, with a narrower bandgap energy. These VBM changes indicate that the Pb vacancies influenced the energy level changes to a greater extent than the Cs vacancies, in agreement with DFT calculations.[41] Moreover, the reduction in the bandgap energy of the CPB NCs on treatment with Ag NCs is consistent with DFT calculations and the red-shifted PL spectrum.

Therefore, experimentation confirmed DDS-based phenomena (targeting, delivery, and release) in the inorganic-material system under investigation, as predicted by theoretical calculations. After the attachment of Ag NCs to the surface of the CPB NCs via Coulombic interactions, the Ag NCs underwent ionization, followed by diffusion into the Pb vacancy in CPB NCs (Figure 5e).[42,43] The ionization and diffusion of Ag NCs could be elucidated using the Hume–Rothery rule and electronic configurations. The Pb atoms in the CPB NCs satisfy three conditions of the Hume–Rothery rule for a solid solution; the atomic radius difference of Pb and Ag is less than 15% (129 pm for Ag^+ and 133 pm for Pb^{2+}), the electronegativity of Pb is similar to that of Ag (≈1.9), and both Ag and Pb exhibit a face-centered cubic crystal-structure. Furthermore, Ag^+ exhibits an outermost-shell configuration of nd^{10}, which favors interactions with the halide ion *p* orbitals in perovskite structures, narrowing the bandgap.[44] This can be used to explain the bandgap reduction in CPB NCs after Ag treatment. An nd^{10} outermost shell is formed by the loss of a single electron from Ag^0 ($[Kr]\ 4d^{10}5s^1$); Therefore, Ag undergoes facile ionization to Ag^+, and subsequently diffuses into the B-sites of the perovskite structure, leading to morphology changes (clean-edged cubic shapes).[14,28,38,45,46]

Subsequently, we empirically confirmed that the DDS-inspired remedy increases the stability of the system, by charge-balance adjustment and structural rearrangement. Since these defects, inducing structural distortions of tilting/rotating axis in CPB NCs, are typically generated by a non-uniform charge distribution in the perovskite structure, charge relaxation and vacancy-filling can stabilize the system. Here, it was investigated that Ag ions passivate the defects and reduce polarized charges in the CPB NCs (Figure S1, Supporting Information), generating ordered surfaces (Figure 3c). In addition, this transition to clean surfaces increased the surface-ligand density. According to Fourier-transform infrared spectroscopy, the ligand density of the CPB-Ag (5d) NCs was considerably greater than that of the as-synthesized CPB NCs (details are provided in Discussion S3 and Figures S7–S9, Supporting Information). Consequently, the colloidal stability of the CPB NCs improved on Ag NC addition (Figure 4a), and the CPB-Ag NCs showed stable PL characteristics (Figure S10, Supporting Information). Therefore, the proposed DDS-inspired strategy prevents defect-structure exacerbation, similar to the

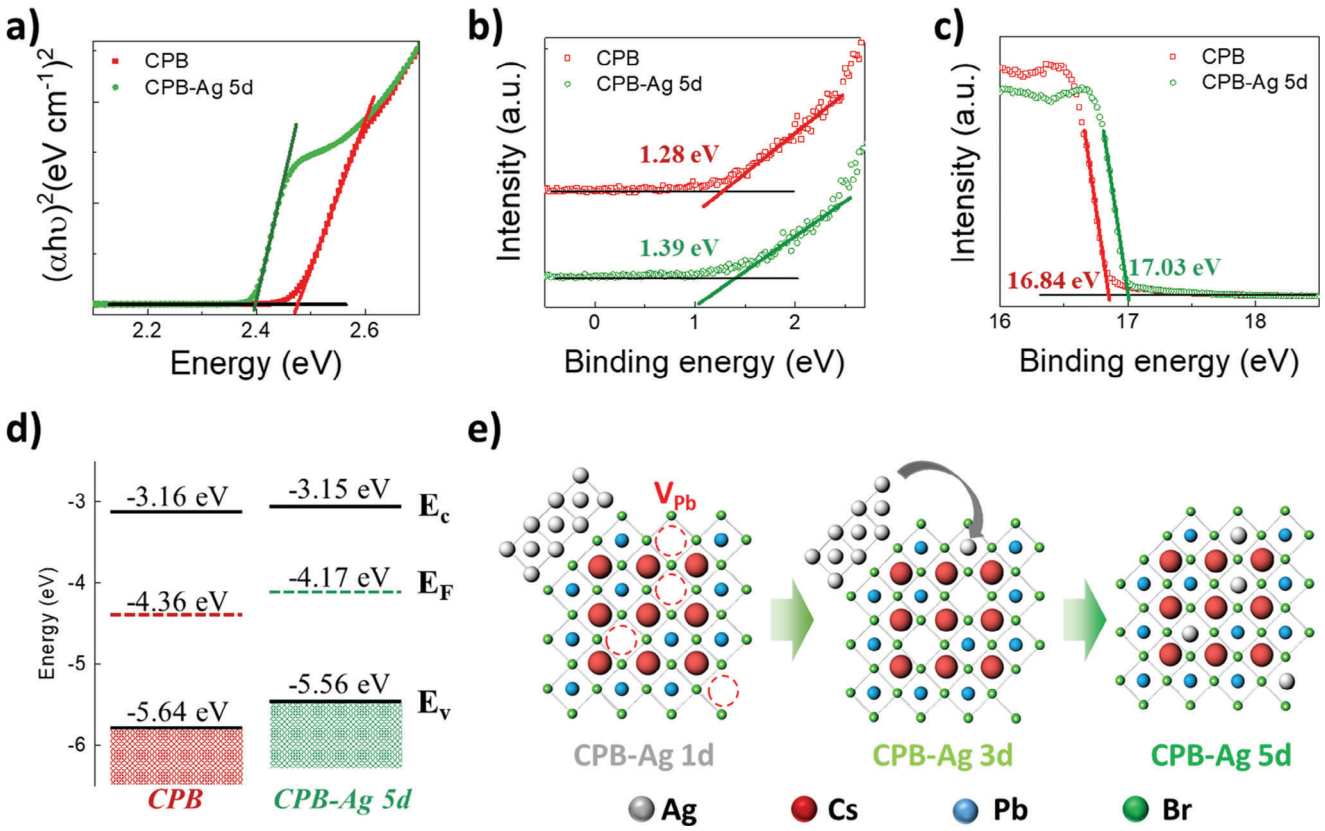

Figure 5. a) Tauc-plot absorbance spectra of the CPB (red) and CPB-Ag NCs (5 days, dark green). UPS profiles of the b) valence band and c) secondary electron cutoff of CPB and CPB-Ag NC thin films (UV excitation by He I = 21.22 eV). Schematic illustration of the d) energy levels (dashed line = Fermi energy level) and e) Ag NC-doping in CPB NCs.

prevention of illness in the human body by vaccination or inoculation.

Then, as shown in **Figure 6**, perovskite NC-based WLEDs were used to confirm the effects of the Ag drugs on the as-synthesized CPB NCs. Emissive perovskite NCs, showing green- and red-PL emission, were designed for experimentation. To form red-emissive perovskite NCs, the Br^- atoms in the CPB-Ag NCs were replaced with I^-, reducing the optical bandgap of the perovskite system (Figure 6a).[47,1] $CsPbBr_{3-x}I_x$-(CPI) Ag perovskite NCs, used as red-emissive color filters, were prepared by mixing NaI solutions with CPB-Ag NC dispersions (the details are described in Methods).[4,48] As shown in Figure 6b, the color changes of the CPB-Ag NC dispersions in situ were monitored, upon treatment with NaI solutions. A color change was observed immediately after mixing; moreover, after shaking the dispersions for 10 s, they became red. The DDS effects of Ag treatment worked well even when it was converted to CPI-Ag NCs by anion exchange. It was found that the PL emission of CPI-Ag NCs was maintained for a longer time than the NaI-treated as-synthesized CPB NCs, similar to the Ag-treated CPB results (Figure S11, Supporting Information).

To fabricate green- and red-colored filters, thin films of colloidal CPB-Ag and CPI-Ag NCs were stacked in a layer-by-layer structure on blue LEDs (Figure 6c, left). Both CPB-Ag and CPI-Ag NCs were respectively coated on PET substrates to effectively prevent anion exchange between them (results without PET substrates are described in Figure S12, Supporting Information). The intensity of the blue light gradually reduced on passing through the CPB-Ag and CPI-Ag NC films, and white light appeared on top of the structure (Figure 6c, right). The light spectrum was investigated using PL spectroscopy, as shown in Figure 6d; blue light (at 450 nm) showed the lowest intensity, green emission from the CPB-Ag NC films showed intermediate intensity, while red emission from the CPI-Ag NC films showed the highest intensity over a wider wavelength range. The white balance of the WLED was estimated using the power of the applied voltage, concentration of the colloidal perovskite NCs, thickness of the films, and so on (Figure 6d, inset). Additionally, the light spectrum was calculated and marked in Commission Internationale de l'éclairage (CIE) coordinates (Figure 6e). The coordinates for the emitted white light were located at the center of the red–green–blue triangle within the CIE color space; the coordinates for the wavelengths of 450, 520, and 620 nm were (0.15, 0.02), (0.07, 0.83), and (0.69, 0.31), respectively.[49] CIE coordinates of both as-synthesized and CPB-Ag (5d) NC-based structures are optimized at (0.30, 0.30), which represents bright white-color emission (black dot). Subsequently, we examined the sustainability of color purity by tracking changes in the CIE coordinates after 48 h. Interestingly, while the position of the WLEDs (without Ag NC-treatments) is shifted to a non-white region (blue dot), the WLEDs (with Ag NC-treatments) maintained the emission of white light with coordinates at (0.29, 0.31; red dot).

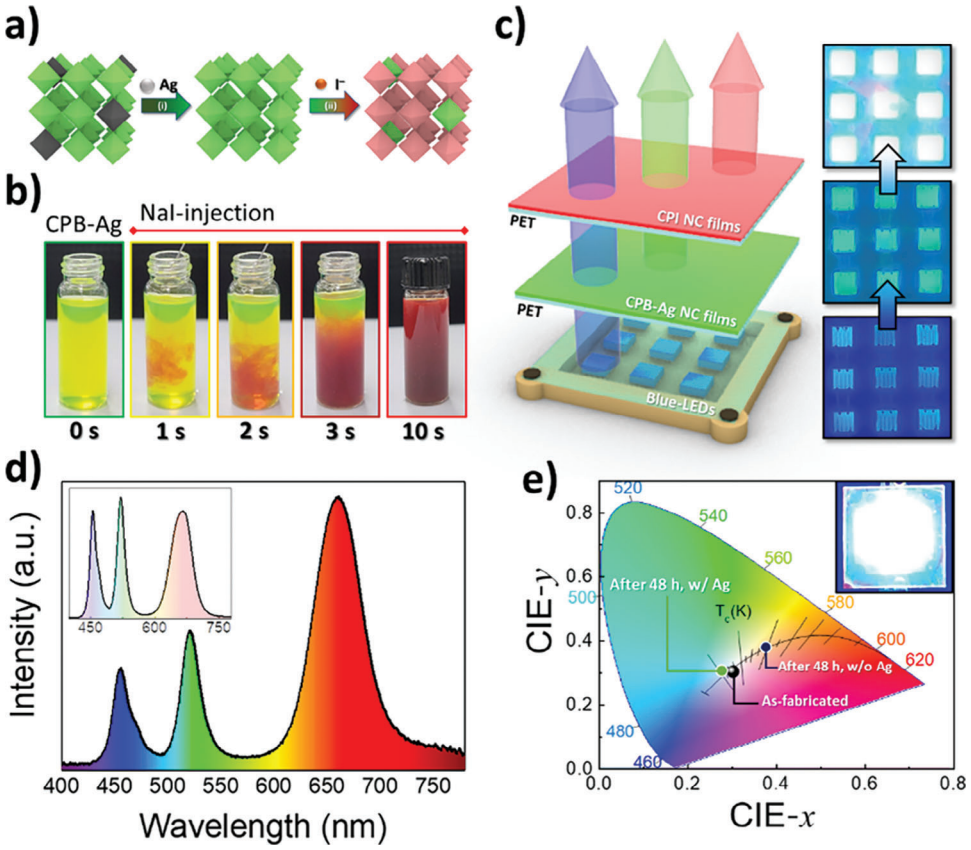

Figure 6. a) Illustration of the synthesis of $CsPbBr_{3-x}I_x$ NCs [(i) = Ag treatment and (ii) NaI treatment]. b) Image capture of the anion-exchange video. c) Schematic representation of white light-emitting diode (WLED) structures (left) and photographs of the top-view of the LEDs (right; λ_{ex}= 450 nm). d) PL spectrum of the downconverter layers (inset = different white emissive spectra). e) CIE color coordinates (black dot = this study). Inset = photograph of the WLEDs at 6 V.

3. Conclusion

In this work, we developed a DDS-inspired strategy for the structural recovery of CPB NCs, using CPB NCs as the substrate and Ag NCs as the drug. Treatment with Ag NCs enabled CPB NCs to recover their original structure, improving their optical properties and structural stability. Theoretical simulations and empirical analyses were used to investigate different aspects of the DDS-type process, including circulation, delivery to target sites, recovery, and prevention. Ag ions, transported to the Br atoms on the CPB NC surface, diffused to Pb vacancies and healed the trap states, preventing structural degradation and the deterioration of properties. The proposed strategy, representing a convergence of pharmacology and materials engineering, could enable a fundamental understanding of materials science and contribute immensely to industrial research on perovskite-based solar cells, displays, and image sensors.

4. Experimental Section

Materials: OA (tech., 90%), oleylamine (OAm, 70%), lead (II) bromide (>98%), and 2-propanol (anhydrous, 99.5%) were purchased from Sigma–Aldrich. Silver nitrate ($AgNO_3$, ACS, >99.9%, metal basis), cesium bromide (CsBr, 99.999%, metal basis), sodium iodide (NaI, 99+%, dry wt., water <1.0%), and dimethyl sulfoxide (DMSO, anhydrous, 99.8%) were purchased from Alfa Aesar. Toluene (99.5%) and ethanol (EtOH, 95.0%) were purchased from Samchun Chemicals.

Preparation of $CsPbBr_3$ Perovskite NCs: CsBr (27.2 mg) and $PbBr_2$ (59.0 g) were dissolved in 4 mL of DMF. Subsequently, 2 mL of this solution was mixed with 0.2 mL of OA and 0.1 mL of OAm and injected into 50 mL of toluene in a flask containing a stirring bar. After stirring for more than 1 min, a green color appeared. This solution was then blended with 30 mL of methyl acetate and centrifuged at 8000 rpm for 3 min. The synthesized $CsPbBr_3$ NC powder was dispersed in hexane to a concentration of 10 mg mL^{-1}.

Preparation of Ag NCs (with a size of 3–5 nm): $AgNO_3$ (1.7 g) was placed in a 100 mL 3-necked flask and blended with OA (45 mL) and OAm (5 mL). Subsequently, this container was de-gassed for more than 90 min at 70 °C, and then filled with nitrogen gas. Next, the flask was heated to 180 °C at a rate of 1 °C min^{-1}. After attaining a temperature of 180 °C, the heating mantle was removed, and the solution was cooled to 25 °C. The obtained Ag NC dispersion was divided into two 50 mL centrifuge tubes, followed by the addition of toluene (20 mL) to each part. The solutions were then centrifuged at 8000 rpm for 1 min, followed by the addition of EtOH, and centrifugation at 5000 rpm for 5 min. Subsequently, the Ag NCs formed were collected and dispersed in toluene. After purification twice, the Ag NCs were re-dispersed in hexane.

Anion Exchange Process and the Fabrication of WLEDs: The CPI NCs were prepared using previously reported anion exchange method. The NaI solution for anion exchange was dissolved in 2-propanol at a concentration of 30 mM. The NaI solution was mixed with the Ag-treated CPB NC dispersions at a ratio of 1:15 v/v%. The red-emissive dispersions were

spin-coated on a poly(ethylene terephthalate) (100 µm, SKC chemicals) at 500 rpm for 30 s and the film was annealed at 70 °C for 2 min. The processes of the deposition and annealing were repeated several times to obtain sufficient absorbances. The green-emissive films were obtained by conducting the same processes with Ag-CPB NCs. By stacking the films on the blue-LEDs, WLEDs were obtained.

Characterization: The chemical properties of the NCs were investigated by XPS (X-TOOL, ULVAC-PHI), and optical bandgap energies were estimated using UPS (Ultra DLD, Korea Basic Science Institute). The surface ligands were examined using a Fourier-transform infrared (FT-IR) spectrometer (Nicolet is10 and iz10, Thermo Scientific) with an integrating sphere (Pike Technologies). The compositional properties of the samples were measured using EDX (S-4300, Hitachi), while the morphological properties were measured using TEM (Tecnai G2 F30, FEI, Korea Basic Science Institute). For structural analysis, XRD (SmartLab, Rigaku) and GI-WAXS (D8 DISCOVER, Bruker) were used, along with a 2-D detector (VANTEC500, resolution = 1024 × 1024 pixel) with a detector distance of 149.3 mm.

The photoluminescence (PL) was investigated using a PL spectrometer (FP-8500, JASCO) and UV-vis–NIR spectrophotometer (V-770, JASCO), while a confocal microscope (MicroTime-200, Picoquant, Germany) with a 40x objective was used for TR-PL analysis. A single-mode pulsed diode laser (375 nm with a pulse width of 30 ps and average power <1 µW) was used as an excitation source, and a dichroic mirror (Z375RDC, AHF), long-pass filter (HQ405lp, AHF), band-pass filter (500–550 nm, Thorlabs) and avalanche photodiode detector (PDM series, MPD) were used to collect emission photons from the samples. PL lifetime images, consisting of 200 × 200 pixels, were recorded using the time-tagged time-resolved data acquisition method. The acquisition time of each pixel was 1 ms. The Symphotime-64 software (Ver. 2.2) was used for the exponential fitting of the obtained emission decays.

Simulation Methods: First-principles calculations using a plane-wave basis set and projector augmented wave potential, as implemented in the Vienna Ab-initio Simulation Package, were used to estimate the electronic structures and adsorption energy.[50,51] The generalized gradient approximation within the modified Perdew–Burke–Ernzerhof (PBEsol) functional was used as the exchange-correlation potential.[52] A kinetic energy cutoff of 400 eV was considered. Additionally, 4 × 4 × 4 *k*-points were used for a 3 × 3 × 3 supercell and 4 × 8 × 1 *k*-points were used for a $\sqrt{2} \times \sqrt{2} \times 2$ supercell. All the CPB supercell structures were optimized with/without an Ag atom, until a force criterion of 0.03 eV $Å^{-1}$.

To calculate the adsorption energy, a vacuum level of 15 Å was considered along the z-axis in the $\sqrt{2} \times \sqrt{2} \times 2$ supercell. The energy was calculated using the following equation: $E_{ads} = E^{relax}_{CPB+Ag} - (E^{relax}_{CPB} - E_{Ag})$, where E^{relax}_{CPB+Ag} and E^{relax}_{CPB} represent the calculated total energy of the relaxed-slab CPB structure with and without adsorbed Ag, respectively, while E_{Ag} indicates the energy of Ag in the gaseous phase. Moreover, based on previously published information, the surface of CPB was considered to be a (110) plane.[6]

Notably, CPB exhibits a strong spin-orbit coupling (SOC) effect. The energy bandgap estimated using SOC is half the value estimated using PBE. Therefore, additional approximations (such as the hybrid or mBJ functional) should be included, to increase the bandgap. However, as this computational task is time-consuming in the model used here, the SOC effect was not considered in calculations.

Supporting Information

Supporting Information is available from the Wiley Online Library or from the author.

Acknowledgements

S.J. and J.A. contributed equally to this work. This research was supported by the Creative Materials Discovery Program through the National Research Foundation of Korea (NRF) funded by the Ministry of Science and ICT (NRF-2018M3D1A1059001), the Basic Science Research Program through the National Research Foundation of Korea (NRF) funded by the Ministry of Science, ICT and Future Planning (2022R1A2C4001517), Materials Innovation Project (NRF-2021M3H4A3026733), and the National Research Foundation of Korea (NRF) grant funded by the Korea government (MSIT) (No. 2022R1A2C2005943).

Conflict of Interest

The authors declare no conflict of interest.

Data Availability Statement

The data that support the findings of this study are available in the supplementary material of this article.

Keywords

all inorganic perovskite, cesium lead halide perovskite nanocrystal, drug-delivery system, perovskite healing, silver nanocrystal

Received: August 16, 2023
Revised: November 19, 2023
Published online:

[1] Y. J. Yoon, K. T. Lee, T. K. Lee, S. H. Kim, Y. S. Shin, B. Walker, S. Y. Park, J. Heo, J. Lee, S. K. Kwak, G.-H. Kim, J. Y. Kim, *Joule* **2018**, *2*, 2105.
[2] B. Sun, A. Johnston, C. Xu, M. Wei, Z. Huang, Z. Jiang, H. Zhou, Y. Gao, Y. Dong, O. Ouellette, X. Zheng, J. Liu, M.-J. Choi, Y. Gao, S.-W. Baek, F. Laquai, O. M. Bakr, D. Ban, O. Voznyy, F. P. García De Arquer, E. H. Sargent, *Joule* **2020**, *4*, 1542.
[3] J. Ye, M. M. Byranvand, C. O. Martínez, R. L. Z. Hoye, M. Saliba, L. Polavarapu, *Angew. Chemie – Int. Ed.* **2021**, *60*, 21636.
[4] J. Ahn, Y. M. Lee, J. Jeon, J. Bang, S. Jeon, H. K. Woo, S. Y. Lee, J. H. Bae, W. Kim, Y. K. Choi, S. J. Kim, S. J. Oh, *Adv. Mater. Technol.* **2022**, *7*, 2200031.
[5] Y. Liu, F. Li, Q. Liu, Z. Xia, *Chem. Mater.* **2018**, *30*, 6922.
[6] S. Jeon, M.-C. Jung, J. Ahn, H. K. Woo, J. Bang, D. Kim, S. Y. Lee, H. Y. Woo, J. Jeon, M. J. Han, T. Paik, S. J. Oh, *Nanoscale Horiz.* **2020**, *5*, 960.
[7] Y. Tidhar, E. Edri, H. Weissman, D. Zohar, G. Hodes, D. Cahen, B. Rybtchinski, S. Kirmayer, *J. Am. Chem. Soc.* **2014**, *136*, 13249.
[8] B. Akbali, G. Topcu, T. Guner, M. Ozcan, M. M. Demir, H. Sahin, *Phys. Rev. Mater.* **2018**, *2*, 034601.
[9] H. Kim, J. S. Han, S. G. Kim, S. Y. Kim, H. W. Jang, *J. Mater. Chem. C* **2019**, *7*, 5226.
[10] A. A. Leonard, B. T. Diroll, N. C. Flanders, S. Panuganti, A. Brumberg, M. S. Kirschner, S. A. Cuthriell, S. M. Harvey, N. E. Watkins, J. Yu, M. R. Wasielewski, M. G. Kanatzidis, W. R. Dichtel, X. Zhang, L. X. Chen, R. D. Schaller, *ACS Nano* **2023**, *17*, 5306.
[11] C. Zheng, A. Liu, C. Bi, J. Tian, *Wuli Huaxue Xuebao/Acta Phys. – Chim. Sin.* **2021**, *37*, 2007084.
[12] Z. Xu, Z. Liu, Y. Huang, G. Zheng, Q. Chen, H. Zhou, *J. Mater. Chem. C* **2017**, *5*, 5810.
[13] J. Kang, L.-W. Wang, *J. Phys. Chem. Lett.* **2017**, *8*, 489.
[14] Q. Chen, L. Chen, F. Ye, T. Zhao, F. Tang, A. Rajagopal, Z. Jiang, S. Jiang, A. K.-Y. Jen, Y. Xie, J. Cai, L. Chen, *Nano Lett.* **2017**, *17*, 3231.
[15] M. N. Islam, M. A. Hadi, J. Podder, *AIP Adv.* **2019**, *9*, 125321.

[16] M. Z. Rahaman, A. K. M. Akther Hossain, *RSC Adv.* **2018**, *8*, 33010.
[17] C.-H. Kuan, S.-H. Yang, *Mater. Adv.* **2022**, *3*, 7824.
[18] F. Krieg, S. T. Ochsenbein, S. Yakunin, S. Ten Brinck, P. Aellen, A. Süess, B. Clerc, D. Guggisberg, O. Nazarenko, Y. Shynkarenko, S. Kumar, C.-J. Shih, I. Infante, M. V. Kovalenko, *ACS Energy Lett.* **2018**, *3*, 641.
[19] V. Naresh, N. Lee, *ACS Appl. Nano Mater.* **2020**, *3*, 7621.
[20] J. Martynczuk, F. Liang, M. Arnold, V. Sepelák, A. Feldhoff, *Chem. Mater.* **2009**, *21*, 1586.
[21] Y. Yang, Y. Li, W. Gong, H. Guo, X. Niu, *Colloids Surfaces A Physicochem. Eng. Asp.* **2023**, *663*, 131083.
[22] X. Huang, H. Li, C. Zhang, S. Tan, Z. Chen, L. Chen, Z. Lu, X. Wang, M. Xiao, *Nat. Commun.* **2019**, *10*, 1163.
[23] T. L. M. Ten Hagen, M. R. Dreher, S. Zalba, A. L. B. Seynhaeve, M. Amin, L. Li, D. Haemmerich, *Commun. Bio.* **2021**, *4*, 920.
[24] J. K. Patra, G. Das, L. F. Fraceto, E. Vangelie, R. Campos, P. Rodriguez, L. Susana, A. Torres, L. Armando, D. Torres, R. Grillo, *J. Nanobiotechnol.* **2018**, *71*, 16.
[25] M. Karimi, P. Sahandi Zangabad, S. Baghaee-Ravari, M. Ghazadeh, H. Mirshekari, M. R. Hamblin, *J. Am. Chem. Soc.* **2017**, *139*, 4584.
[26] L. Kou, Y. D. Bhutia, Q. Yao, Z. He, J. Sun, V. Ganapathy, *Front. Pharmacol.* **2018**, *9*, 1.
[27] F. U. Din, W. Aman, I. Ullah, O. S. Qureshi, O. Mustapha, S. Shafique, A. Zeb, *Int. J. Nanomed.* **2017**, *12*, 7291.
[28] S. Chen, X. Liu, Z. Wang, W. Li, X. Gu, J. Lin, T. Yang, X. Gao, A. K. K. Kyaw, *Adv. Energy Sustain. Res.* **2021**, *2*, 2000099.
[29] Y. Wang, Z. Lv, Q. Liao, H. Shan, J. Chen, Y. Zhou, L. Zhou, X. Chen, V. A. L. Roy, Z. Wang, Z. Xu, Y.-J. Zeng, S.-T. Han, *Adv. Mater.* **2018**, *30*, 1800327.
[30] H. Kim, M.-J. Choi, J. M. Suh, J. S. Han, S. G. Kim, Q. V. Le, S. Y. Kim, H. W. Jang, *NPG Asia Mater* **2020**, *12*, 21.
[31] D. J. Keeble, J. Wiktor, S. K. Pathak, L. J. Phillips, M. Dickmann, K. Durose, H. J. Snaith, W. Egger, *Nat. Commun.* **2021**, *12*, 5566.
[32] S. Tan, M. Erol, A. Attygalle, H. Du, S. Sukhishvili, *Langmuir* **2007**, *23*, 9836.
[33] J. Ahn, S. Jeon, W. S. Lee, H. K. Woo, D. Kim, J. Bang, S. J. Oh, *J. Phys. Chem. C* **2019**, *123*, 18087.
[34] S. Jeon, J. Ahn, H. Kim, H. K. Woo, J. Bang, W. S. Lee, D. Kim, M. A. Hossain, S. J. Oh, *J. Phys. Chem. C* **2019**, *123*, 11001.
[35] M. A. Hossain, S. Jeon, J. Ahn, H. Joh, J. Bang, S. J. Oh, *J. Ind. Eng. Chem.* **2019**, *73*, 214.
[36] C. K. Ng, W. Yin, H. Li, J. J. Jasieniak, *Nanoscale* **2020**, *12*, 4859.
[37] J. Liang, P. Zhao, C. Wang, Y. Wang, Y. Hu, G. Zhu, L. Ma, J. Liu, Z. Jin, *J. Am. Chem. Soc.* **2017**, *139*, 14009.
[38] S. Zhou, Y. Ma, G. Zhou, X. Xu, M. Qin, Y. Li, Y.-J. Hsu, H. Hu, G. Li, N. Zhao, J. Xu, X. Lu, *ACS Energy Lett.* **2019**, *4*, 534.
[39] M. Liu, G. Zhong, Y. Yin, J. Miao, K. Li, C. Wang, X. Xu, C. Shen, H. Meng, *Adv. Sci.* **2017**, *4*, 1700335.
[40] Y. Zhao, Y. Wang, J. Duan, X. Yang, Q. Tang, *J. Mater. Chem. A* **2019**, *7*, 6877.
[41] T. Chiba, Y. Hayashi, H. Ebe, K. Hoshi, J. Sato, S. Sato, Y.-J. Pu, S. Ohisa, J. Kido, *Nat. Photonics* **2018**, *12*, 681.
[42] S. Chernousova, M. Epple, *Angew. Chem., Int. Ed.* **2013**, *52*, 1636.
[43] S. Kittler, C. Greulich, J. Diendorf, M. Köller, M. Epple, *Chem. Mater.* **2010**, *22*, 4548.
[44] Z. Xiao, Y. Zhou, H. Hosono, T. Kamiya, N. P. Padture, *Chem. – A Eur. J.* **2018**, *24*, 2305.
[45] M. Jahandar, J. H. Heo, C. E. Song, K.-J. Kong, W. S. Shin, J.-C. Lee, S. H. Im, S.-J. Moon, *Nano Energy* **2016**, *27*, 330.
[46] M. Abdi-Jalebi, M. Pazoki, B. Philippe, M. I. Dar, M. Alsari, A. Sadhanala, G. Divitini, R. Imani, S. Lilliu, J. Kullgren, H. Rensmo, M. Grätzel, R. H. Friend, *ACS Nano* **2018**, *12*, 7301.
[47] G. Nedelcu, L. Protesescu, S. Yakunin, M. I. Bodnarchuk, M. J. Grotevent, M. V. Kovalenko, *Nano Lett.* **2015**, *15*, 5635.
[48] J. Ahn, Y. M. Lee, W. Kim, S. Y. Lee, J. H. Bae, J. Bang, S. J. Oh, *ECS J. Solid State Sci. Technol.* **2021**, *10*, 106003.
[49] S. Y. Lee, S. Jeon, J. Ahn, J. Bang, H. K. Woo, K.-J. Lee, B. K. Jung, T. Park, D. Son, J.-P. Ahn, S. J. Oh, *Appl. Surf. Sci.* **2021**, *563*, 150229.
[50] G. Kresse, J. Hafner, *Phys. Rev. B* **1993**, *48*, 13115.
[51] G. Kresse, J. Furthmüller, *Comput. Mater. Sci.* **1996**, *6*, 15.
[52] G. I. Csonka, J. P. Perdew, A. Ruzsinszky, P. H. T. Philipsen, S. Lebègue, J. Paier, O. A. Vydrov, J. G. Ángyán, **2009**, *79*, 155107.